Supplementary Materials for

Facile and Scalable Synthesis of High-Quality Three-Dimensional Imine-Linked Covalent Organic Frameworks via Crystalline Intermediate Transformation

Jiaqiang Liu[a, b, c], Xin Su[a, b, c], Yan Xu[d], Weiwei Tang*[a, b, c], Taimin Yang *[e, f] and Junbo Gong*[a, b, c]

a. State Key Laboratory of Chemical Engineering, School of Chemical Engineering and Technology, Tianjin University, Weijin Road 92, Tian-jin, 300072, China
b. Collaborative Innovation Center of Chemical Science and Engineering, Weijin Road 92, Tianjin, 300072, China
c. Haihe Laboratory of Sustainable Chemical Transformations, Tianjin 300192, China
d. Department of Chemistry, College of Sciences, Northeastern University, Shenyang, Liaoning 110819, China
e. Department of Material and Environmental Chemistry Chemistry (MMK), Stockholm University, Svante Arrhenius väg 16C, Stockholm, SE-10691, Sweden
f. Department of Physics and Astronomy, University of California, Irvine, California 92697, United States

Table of Contents

Synthetic Procedures

Synthesis of CIM-1:

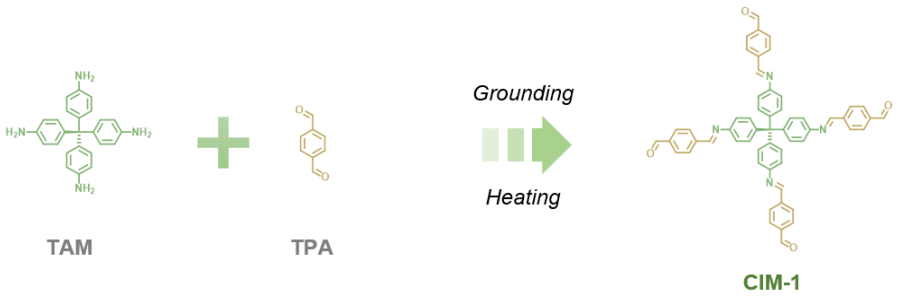

Fig. S1. Synthesis route of CIM-1.

First, 38 mg (0.1 mmol) of tetrakis(4-aminophenyl)methane (TAM) and 134 mg (1.0 mmol) of terephthalaldehyde (TPA) were mixed and ground in a mortar for 30 minutes. It was then transferred to a 25 mL PTFE reactor and heated at 120 °C for 24 hours. After cooling to room temperature, the product was collected, washed with tetrahydrofuran, and dried under vacuum at 120 °C overnight to give a light-yellow powder, CIM-1. To investigate the process details of the synthesis, the samples were extracted and characterized by varying the heating time.

Synthesis of CIM-2:

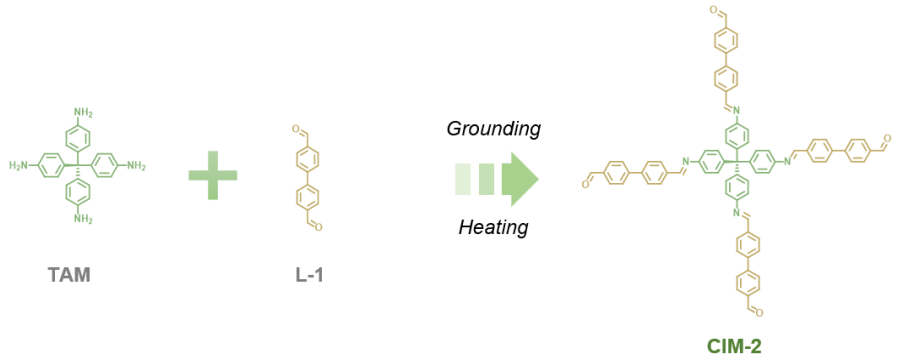

Fig. S2. Synthesis route of CIM-2.

First, 19 mg (0.05 mmol) of TAM and 65 mg(0.31 mmol) 4,4'-biphenyldicarboxaldehyde (L-1) were mixed and ground in a mortar for 30 minutes. It was then transferred to a 25 mL PTFE reactor and heated at 120 °C for 24 hours. After cooling to room temperature, the product was collected, washed with tetrahydrofuran, and dried under vacuum at 120 °C overnight to give a light-yellow powder, CIM-2, in 91% yield.

Synthesis of CIM-3:

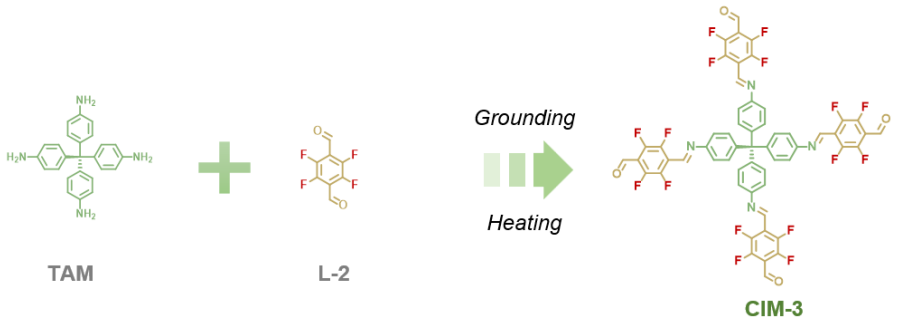

Fig. S3. Synthesis route of CIM-3.

First, 19 mg (0.05 mmol) of TAM and 65 mg (0.32 mmol) of 2,3,5,6-tetrafluoroterephthalaldehyde (L-2) were mixed and ground in a mortar for 30 minutes. It was then transferred to a 25 mL PTFE reactor and heated at 120 °C for 24 hours. After cooling to room temperature, the product was collected, washed with tetrahydrofuran, and dried under vacuum at 120 °C overnight to produce a light-yellow powder, CIM-3, in 87% yield.

Synthesis of CIM-4:

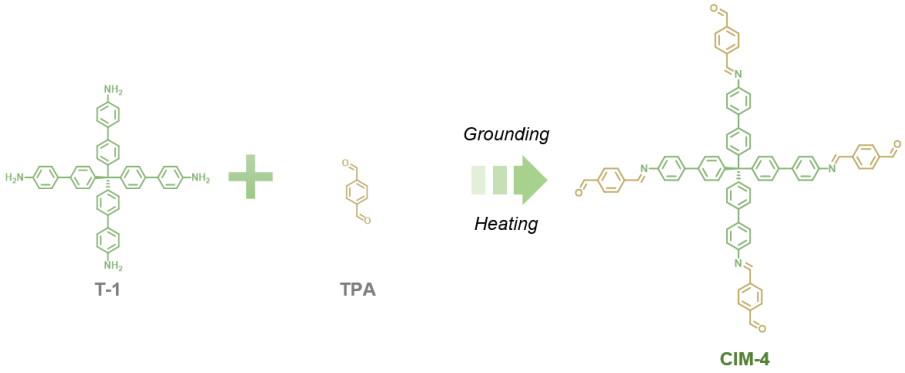

Fig. S4. Synthesis route of CIM-4.

First, 9.8 mg (0.014 mmol) of 4',4''',4''''',4'''''''-methanetetrayltetrakis(([1,1'-biphenyl]-4-amine)) (T-1) and 134 mg (1 mmol) of TPA were mixed and ground in a mortar for 30 minutes. It was then transferred to a 25 mL PTFE reactor and heated at 120 °C for 24 hours. After cooling to room temperature, the product was collected, washed with tetrahydrofuran, and dried under vacuum at 120 °C overnight to produce a light-yellow powder, CIM-4, in 67% yield.

Synthesis of COF-300 from CIM-1:

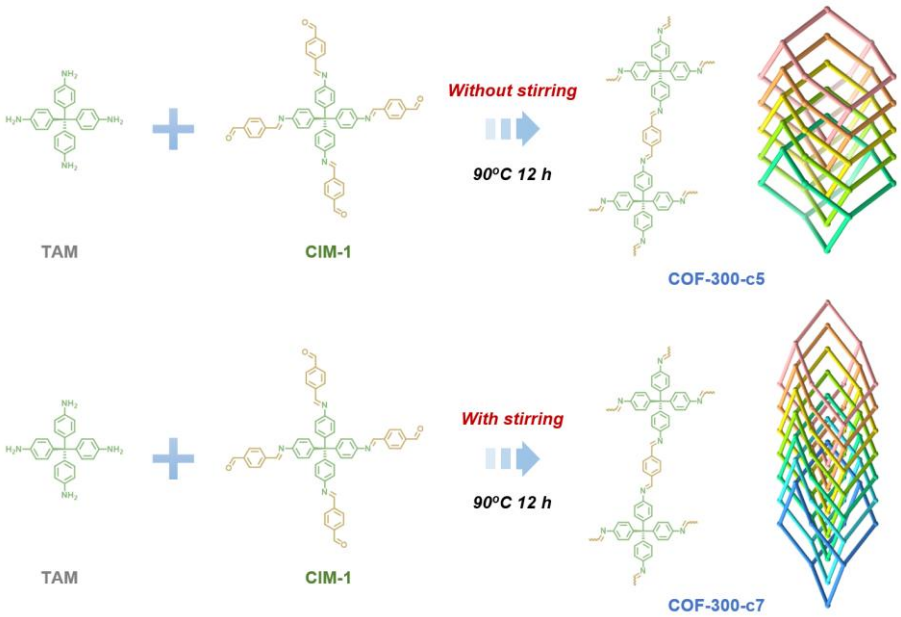

Fig. S5. Synthesis route of COF-300 from CIM-1.

First, 38 mg (0.1 mmol) of TAM and 84.4 mg (0.1 mmol) of CIM-1 were dispersed into 1 ml of solvent mixture ($V_{1,4\text{-Dioxane}}$: V_{water}: $V_{acetic\ acid}$ = 7.5: 5: 1) in a 10 ml pressure resistant glass vial. Directly, the reaction system is heated at 90 °C for 12 hours without stirring. After cooling to room temperature, the solid product was collected, washed with tetrahydrofuran, and dried under vacuum at 120 °C overnight to produce the yellow powder COF-300-c5. Follow the same procedure, the heating process with stirring produced COF-300-c7.

Synthesis of COF-320 from CIM-2:

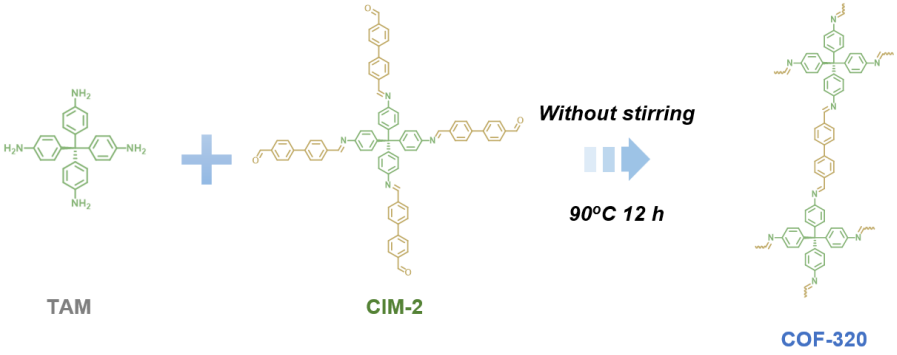

Fig. S6. Synthesis route of COF-320 from CIM-2.

First, 38 mg (0.1 mmol) of TAM and 115 mg (0.1 mmol) of CIM-2 were dispersed into 1 ml of solvent mixture ($V_{1,4\text{-Dioxane}}$: V_{water}: $V_{acetic\ acid}$ = 7.5: 5: 1) in a 10 ml pressure resistant glass vial. Directly, the reaction system is heated at 90 °C for 12 hours without stirring. After cooling to room temperature, the solid product was collected, washed with tetrahydrofuran, and dried under vacuum at 120 °C overnight to produce the yellow powder COF-320 in 86% yield

Synthesis of TJU-300 from CIM-3:

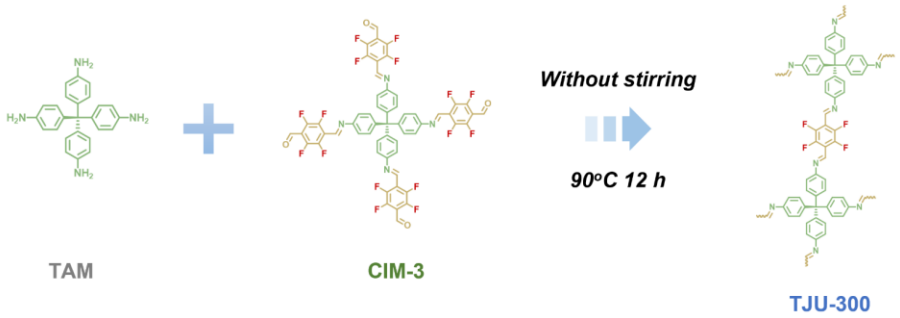

Fig. S7. Synthesis route of TJU-300 from CIM-3.

First, 38 mg of TAM (0.1 mmol) and 113 mg (0.1 mmol) of CIM-3 were dispersed into 1 ml of solvent mixture ($V_{1,4\text{-Dioxane}}$: V_{water}: $V_{acetic\ acid}$ = 7.5: 5: 1) in a 10 ml pressure resistant glass vial. Directly, the reaction system is heated at 90 °C for 12 hours without stirring. After cooling to room temperature, the solid product was collected, washed with tetrahydrofuran, and dried under vacuum at 120 °C overnight to produce the red powder TJU-300 in 89% yield.

Synthesis of TJU-301 from CIM-4:

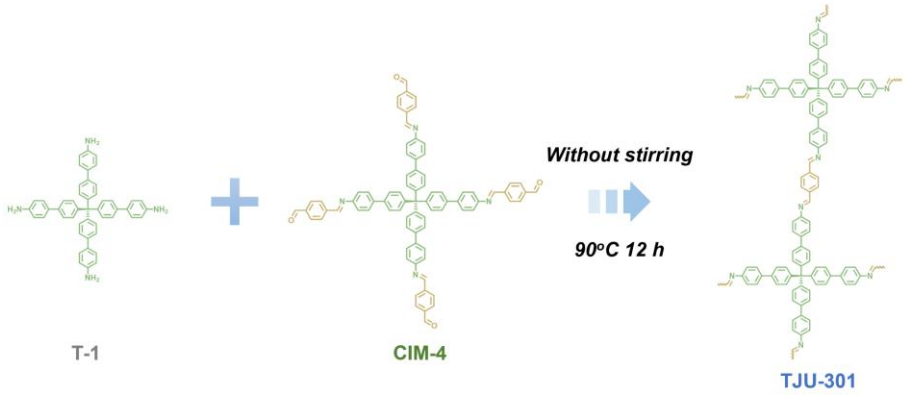

Fig. S8. Synthesis route of TJU-301 from CIM-4.

First, 20 mg (0.03 mmol) of T-1 and 33 mg (0.03 mmol) of CIM-4 were dispersed into 1 ml of solvent mixture ($V_{1,4\text{-Dioxane}}$: V_{water}: $V_{acetic\ acid}$ = 7.5: 5: 1) in a 10 ml pressure resistant glass vial. Directly, the reaction system is heated at 90 °C for 12 hours without stirring. After cooling to room temperature, the solid product was collected, washed with tetrahydrofuran, and dried under vacuum at 120 °C overnight to produce the yellow powder TJU-301 in 82% yield.

Gram-scale synthesis of CIM-1:

The CIM-1 synthesis route was scaled up 100 times. First, 3.8 g (10 mmol) of TAM and 13.4 g (100 mmol) of TPA were mixed and ground in a mortar for 30 minutes. It was then transferred to a 100 mL PTFE reactor and heated at 120 °C for 24 hours. After cooling to room temperature, the product was collected, washed with tetrahydrofuran, and dried under vacuum at 120 °C overnight to produce CIM-1 in 96% yield.

Gram-scale synthesis of COF-300:

Scale up the above COF-300 from CIM-1 synthesis by 2/10/50 times. Only the synthesis parameters were changed as shown in Table S3, and the other steps were the identical as above.

Synthesis of P-1 from CIM-1

First, 84.4 mg of CIM-1 (0.1 mmol) were dispersed into 1 ml of solvent mixture ($V_{1,4\text{-Dioxane}}$: V_{water}: $V_{acetic\ acid}$ = 7.5: 5: 1) in a 10 ml pressure resistant glass vial. Directly, the reaction system is heated at 90 °C for 12 hours without stirring. After cooling to room temperature, the solid product was collected, washed with tetrahydrofuran, and dried under vacuum at 120 °C overnight to produce the sample P-1.

Synthesis procedure of COF-300-CIM$_0$

First, 76.0 mg of TAM (0.2 mmol) and 53.6 mg of TPA (0.4 mmol) were dispersed into 1 ml of solvent mixture ($V_{1,4\text{-Dioxane}}$: V_{water}: $V_{acetic\ acid}$ = 7.5: 5: 1) in a 10 ml pressure resistant glass vial. Directly, the reaction system is heated at 90 °C for 12 hours without stirring. After cooling to room temperature, the solid product was collected, washed with tetrahydrofuran, and dried under vacuum at 120 °C overnight to produce the sample COF-300-CIM$_0$.

Synthesis procedure of COF-300-CIM$_{0.5}$

First, 57.0 mg of TAM (0.15 mmol), 26.8 mg of TPA (0.2 mmol) and 42.2 mg of CIM-1 (0.05 mmol) were dispersed into 1 ml of solvent mixture ($V_{1,4\text{-Dioxane}}$: V_{water}: $V_{acetic\ acid}$ = 7.5: 5: 1) in a 10 ml pressure resistant glass vial. Directly, the reaction system is heated at 90 °C for 12 hours without stirring. After cooling to room temperature, the solid product was collected, washed with tetrahydrofuran, and dried under vacuum at 120 °C overnight to produce the sample COF-300-CIM$_{0.5}$.

Synthesis procedure of COF-300-CIM$_1$

The synthesis of COF-300-CIM$_1$ was consistent with the synthesis of COF-300 from CIM-1 in the main text.

Synthesis of POP-0, POP-1, POP-2, POP-3 or POP-4 (synthesized mechanochemically without thermal treatment)

First, 38 mg of TAM (0.1 mmol) and 26.8 mg of TPA (0.2 mmol) were mixed and ground in a mortar for 30 minutes. It was then dispersed into 1 ml of solvent mixture ($V_{1,4\text{-Dioxane}}$: V_{water}: $V_{acetic\ acid}$ = 7.5: 5: 1) in a 10 ml pressure resistant glass vial. Directly, the reaction system is heated at 90 °C for 0, 1, 3, 6 or 12 hours without stirring. After cooling to room temperature, the solid product was collected, washed with tetrahydrofuran, and dried under vacuum at 120 °C overnight to produce the sample POP-0, POP-1, POP-2, POP-3 or POP-4.

Crystalline intermediate CIM-1

Table S1. Crystallographic data and structure refinement of CIM-1.

Crystal system	Tetragonal
Space group (number)	$I4_1/a$ (88)
a [Å]	24.800
b [Å]	24.800
c [Å]	7.860
α [°]	90
β [°]	90
γ [°]	90
Radiation	Electron (λ=0.0197 Å)
2θ range [°]	0.09 to 1.19 (0.95 Å)
Index ranges	$-26 \le h \le 26$ $-26 \le k \le 26$ $-8 \le l \le 8$
Reflections collected	39751
Independent reflections	1489 R_{int} = 0.4299 R_{sigma} = 0.1725
Completeness to θ = 0.597°	99.5 %
Data / Restraints / Parameters	1489/0/67
Goodness-of-fit on F^2	1.075
Final R indexes [I≥2σ(I)]	R_1 = 0.2696 wR_2 = 0.6413
Final R indexes [all data]	R_1 = 0.3152 wR_2 = 0.6590

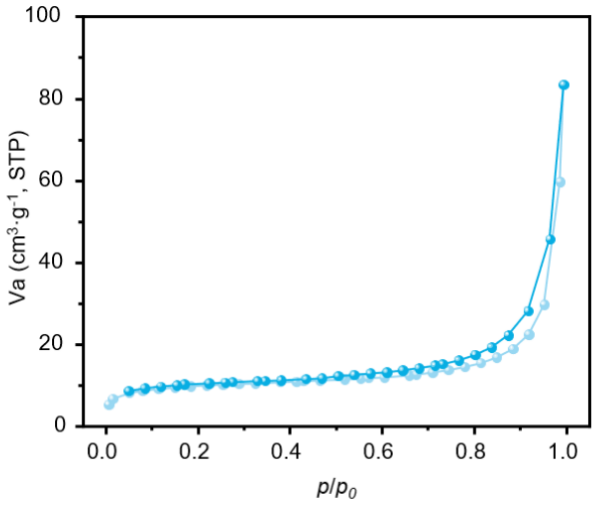

Fig. S9. N_2 adsorption-desorption isotherms of CIM-1.

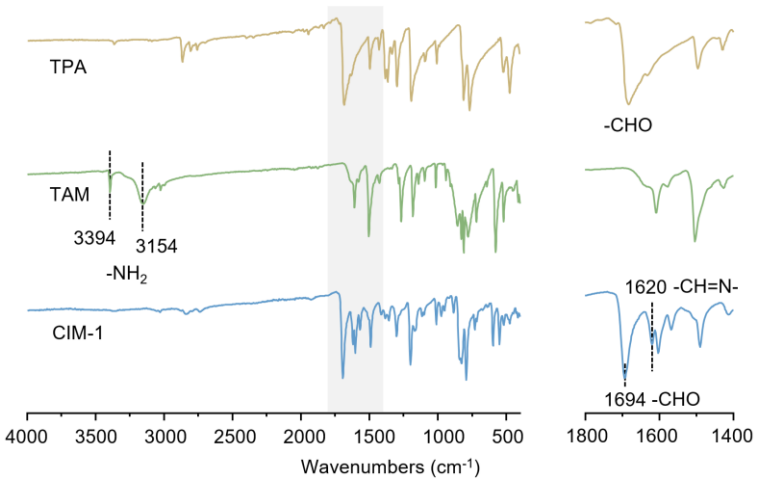

Fig. S10. FTIR spectra of raw materials and CIM-1. The right panel highlights the enlarged pattern of the grey area in the left panel, showing characteristic imine bonding peaks around 1620 cm^{-1} and aldehyde group peaks around 1694 cm^{-1}. The stretching absorption peaks of the amino group evident in TAM at 3394 cm^{-1} and 3154 cm^{-1} were not observed in CIM-1.

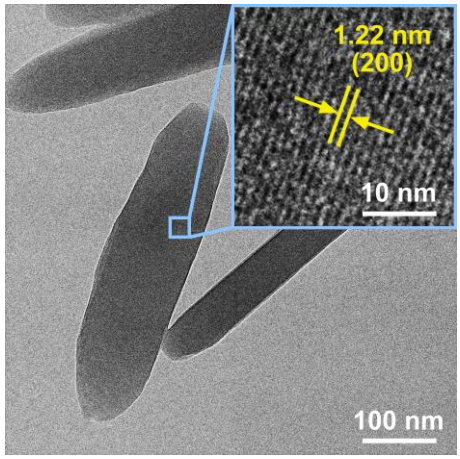

Fig. S11. High resolution transmission electron microscopy image of CIM-1 with the enlarged lattice fringe image (inset) showing clear lattice fringes, confirming the long-range ordered structure of CIM-1.

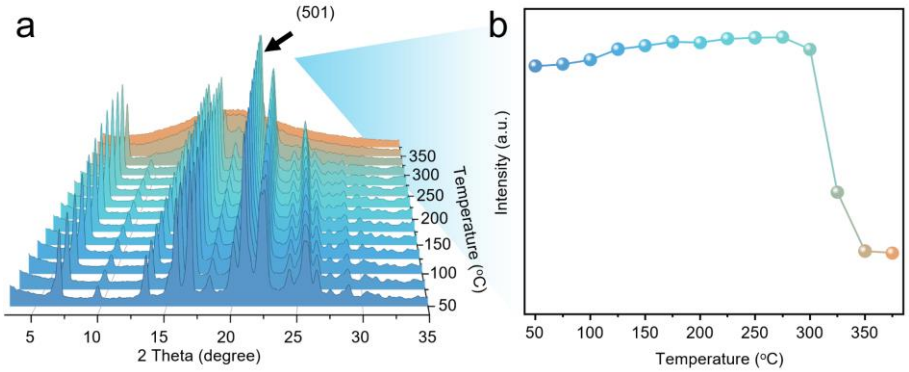

Fig. S12. (a) *In situ* PXRD patterns of CIM-1 that were collected at 25 °C intervals, and(b) the intensity of the diffraction peak corresponding to the (501) crystal plane of CIM-1 varys as a function temperature, suggesting that CIM-1 maintains its crystalline structure at less than 300 °C in air.

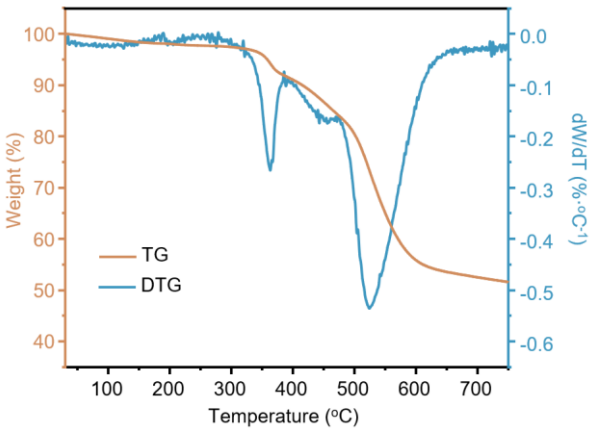

Fig. S13. TGA and DTG plots of CIM-1 registered under a dynamic N_2 atmosphere, showing the good thermal stability of CIM-1 under N_2 atmosphere.

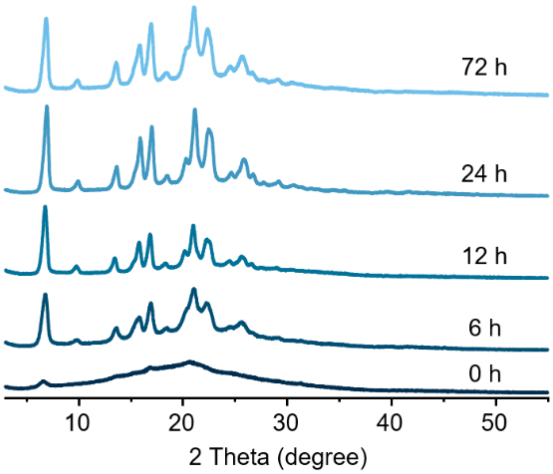

Fig. S14. PXRD patterns collected at different heat treatment times over the course of the CIM-1 synthesis, showing the transformation from amorphous to crystalline CIM-1.

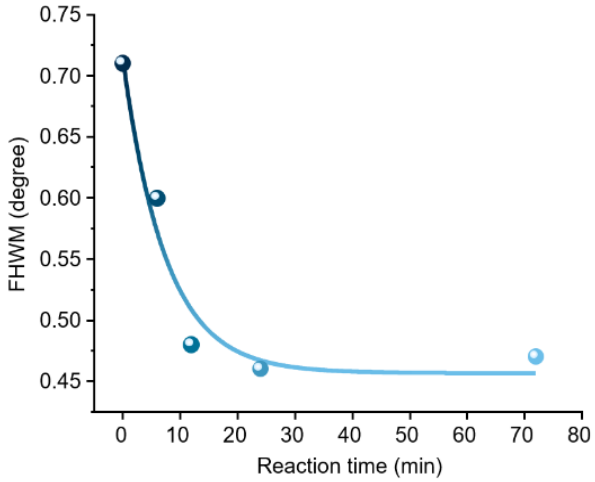

Fig. S15. The full widths at half maximum extracted from time-resolved PXRD patterns at peak (200) in Fig. S14.

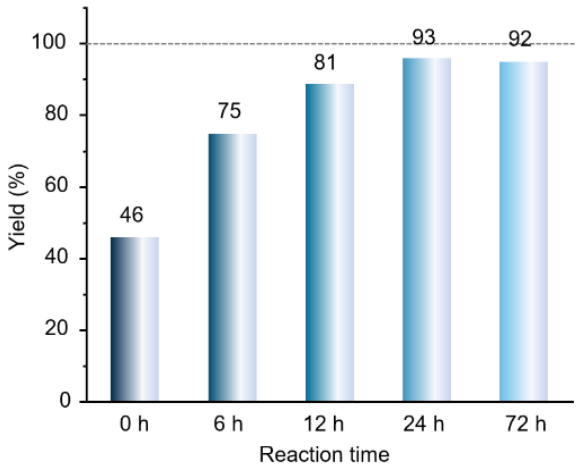

Fig. S16. Product yield of CIM-1 synthesis varying at different heat treatment times.

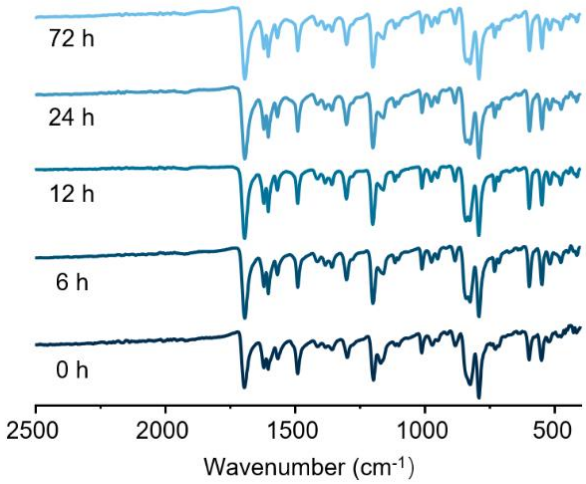

Fig. S17. FTIR spectra collected over the course of CIM-1 synthesis at different heat treatment times.

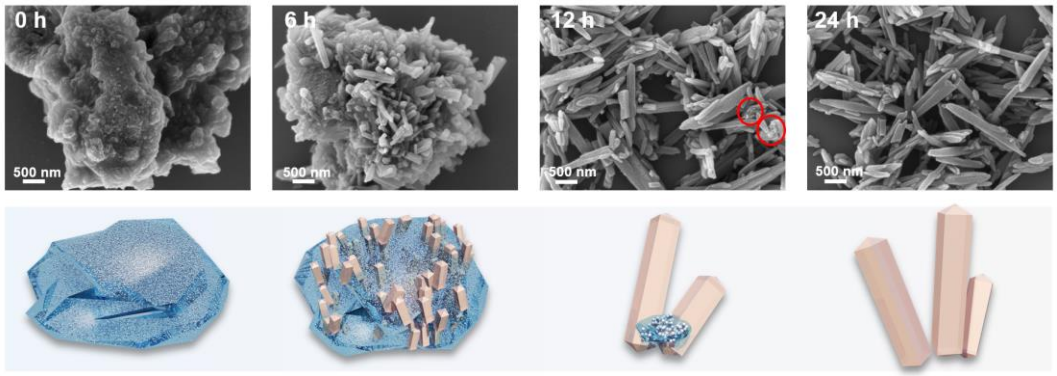

Fig. S18. Time-resolved SEM images collected over the course of CIM-1 synthesis and the corresponding schematic representation of the morphological evolution.

Transformation Process from CIM-1 to COF-300.

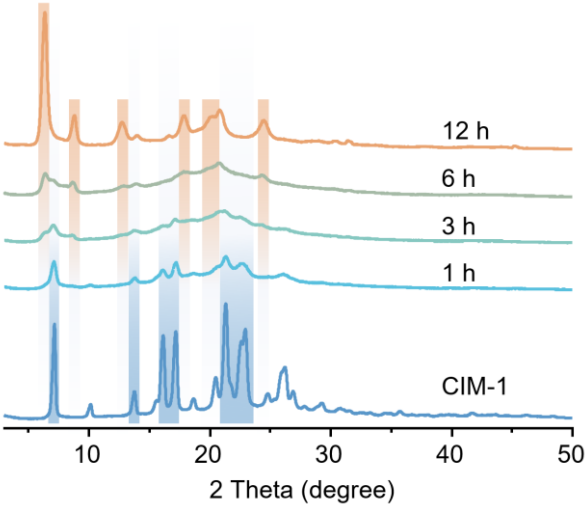

Fig. S19. PXRD patterns collected at different heat treatment times during the transformation of COF-300-c5 from CIM-1.

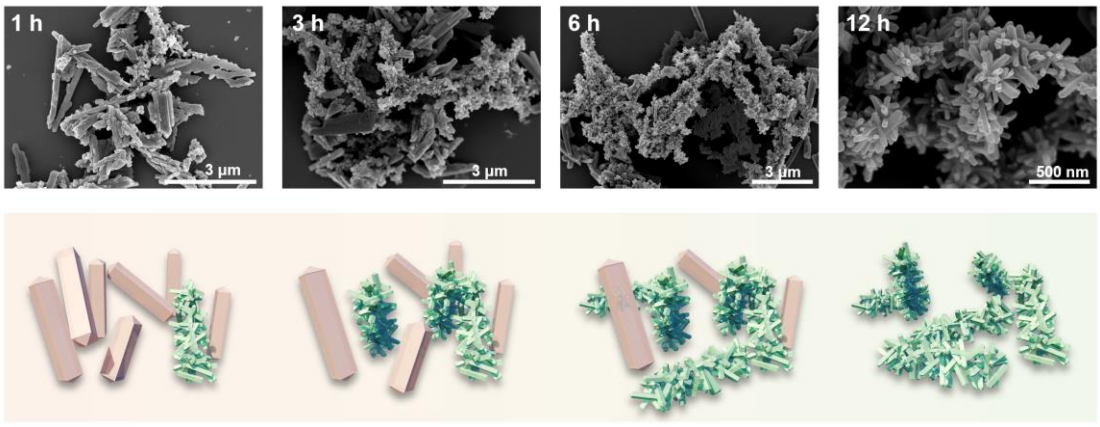

Fig. S20. Time-resolved SEM images collected during the transformation of COF-300-c5 from CIM-1 and the corresponding schematic representation of the morphological evolution.

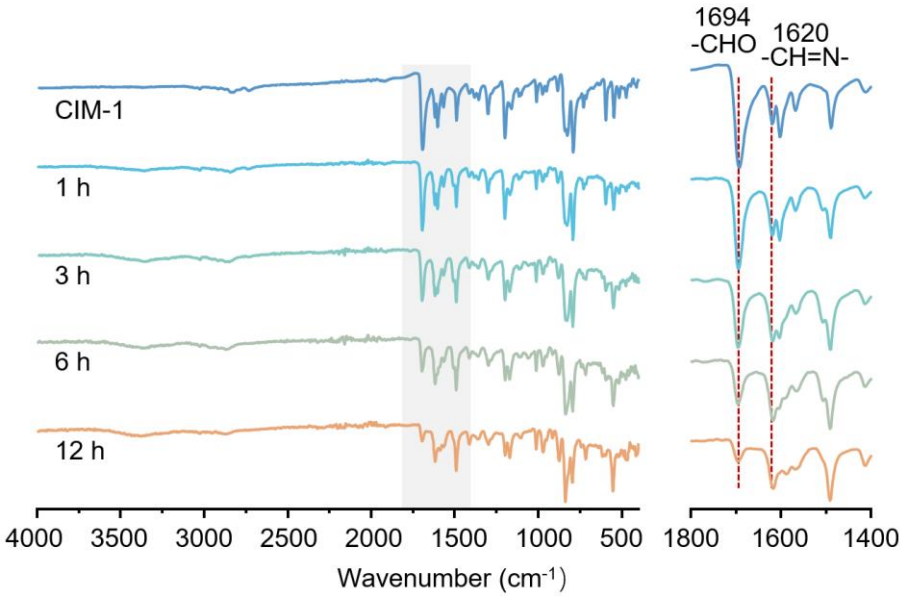

Fig. S21. FTIR spectra collected during the transformation of COF-300-c5 from CIM-1 at different heat treatment times.

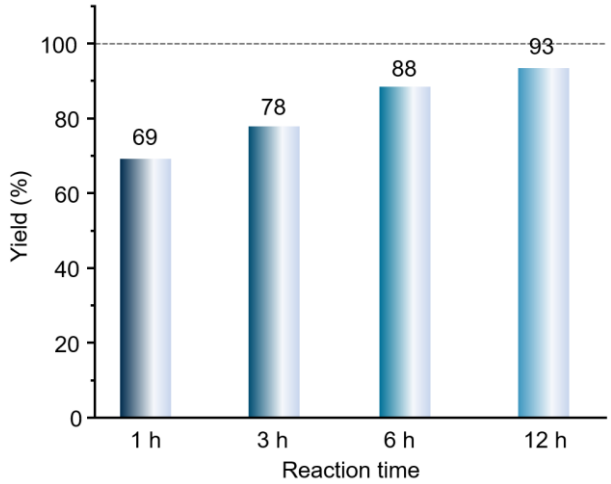

Fig. S22. Product yield of COF-300-c5 synthesis from CIM-1 transformation varying at different heat treatment times.

Table S2. Comparisons of solubility of CIM-1 and raw materials in pure 1,4-dioxane and mixed solvents of 1,4-dioxane, acetic acid, and water.

	TAM	TPA	CIM-1
1,4-Dioxane 100 g	4.119 g	19.916 g	< 0.001g
Mixed solvents （$V_{1,4\text{-Dioxane}}$: V_{water}: $V_{acetic\ acid}$ = 7.5: 5: 1） 100 g	-	-	< 0.001g

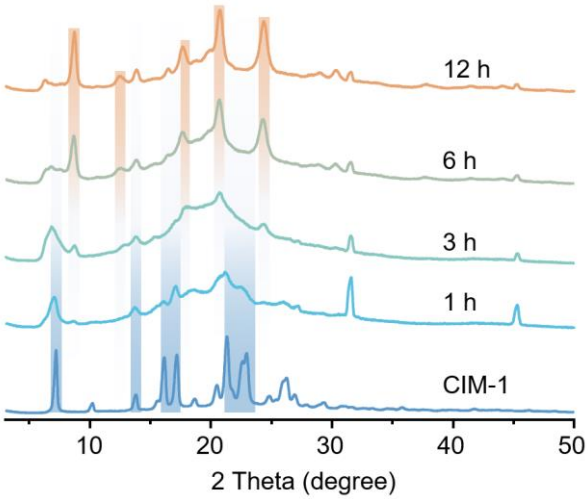

Fig. S23. PXRD patterns collected at different heat treatment times during the transformation of COF-300-c7 from CIM-1.

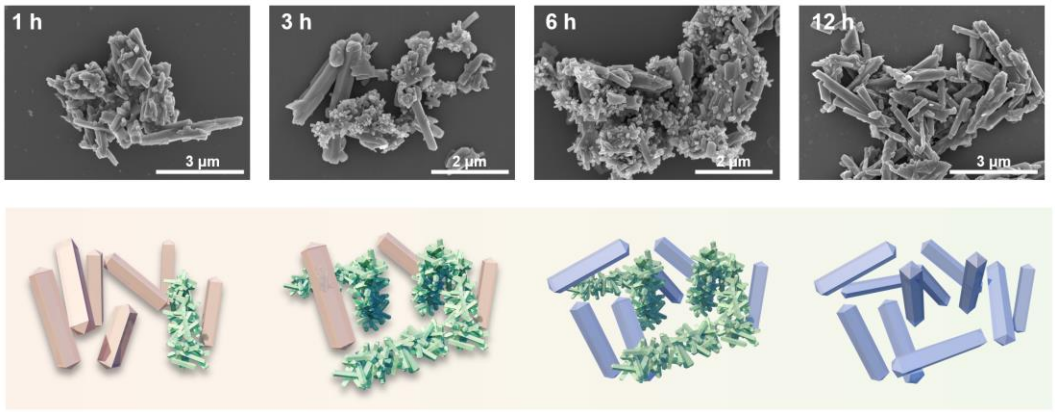

Fig. S24. Time-resolved SEM images collected during the transformation of COF-300-c7 from CIM-1 and the corresponding schematic representation of the morphological evolution.

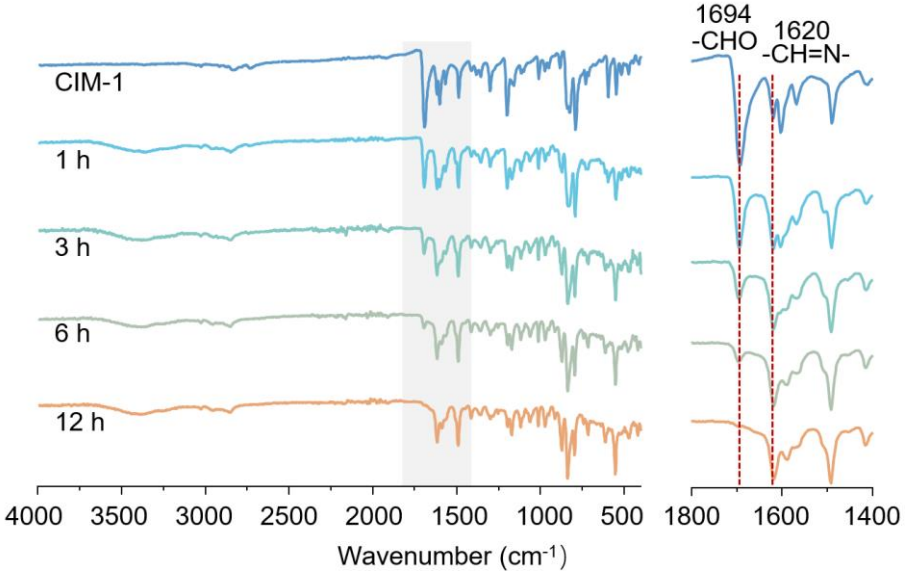

Fig. S25. FTIR spectra collected during the transformation of COF-300-c7 from CIM-1 at different heat treatment times.

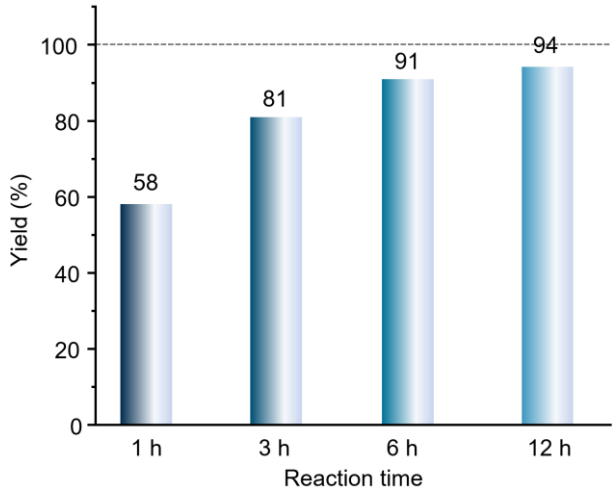

Fig. S26. Product yield of COF-300-c7 synthesis from CIM-1 transformation varying at different heat treatment times.

Scalable Intermediate and COF Synthesis

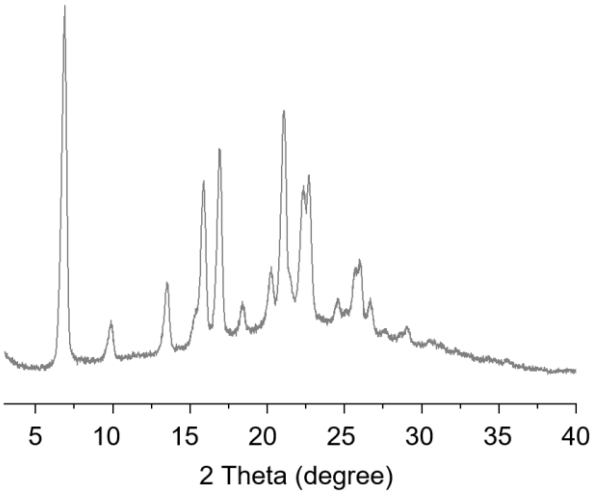

Fig. S27. PXRD pattern of gram-scale production of CIM-1.

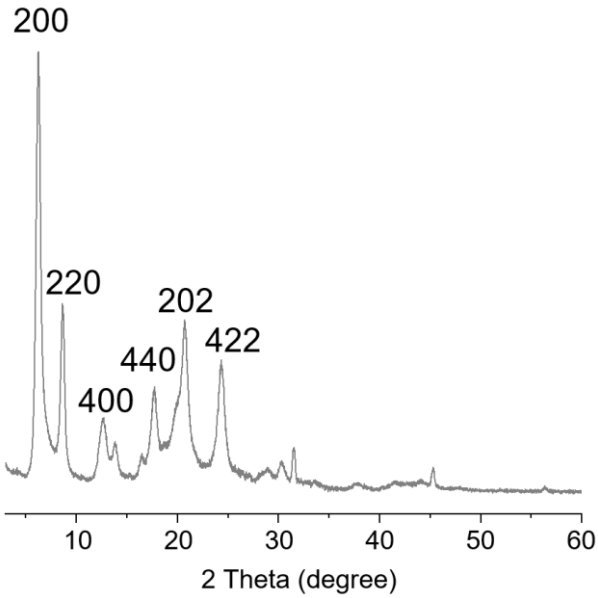

Fig. S28. PXRD pattern of gram-scale production of COF-300.

Table S3. Scale-up synthesis conditions and result of COF-300.

Synthetic Magnification	Mixed solvents /ml	TAM /mg	TAM /mmol	CIM-1 /mg	CIM-1 /mmol	COF-300 obtained /mg	Yield /%
2	1.5	72	0.2	169	0.2	222	92.1
10	10	380	1.0	844	1.0	1143	93.4
50	50	1900	5.0	4220	5.0	5798	94.7

Table S4. Comparisons of reported synthetic condition and results of COF-300 with developed CIM transformation strategy in this work.

Degree of interpenetration	Yield (%)	Temperature (oC)	Space-time Yield (kg m^{-3} day^{-1})	BET surface area (m^2 g^{-1})	Ref.
5-fold	63	120	2.8	1360	(1) J. Am. Chem. Soc. 2009, 131, 4570.
5-fold	-	-	-	756	(2) J. Am. Chem. Soc., 2019, 141, 3298.
7-fold	58	65	2.1	981	(3) Molecules 2022, 27, 8002.
7-fold	92	65	28.9	400	(4) Chem. Mater. 2023, 35, 23, 10070-10077
7-fold	65	65	854.2	-	(5) Nat. Chem. 2023. 15, 841-847.
7-fold	95	Ambient temperature	-	458	(6) Science 2018. 361,48-52.
7-fold	49.8	Ambient temperature	-	-	This work
5-fold	93	90	322	938	This work
7-fold	94	90	-	520	

Crystalline intermediate CIM-2 and COF-320

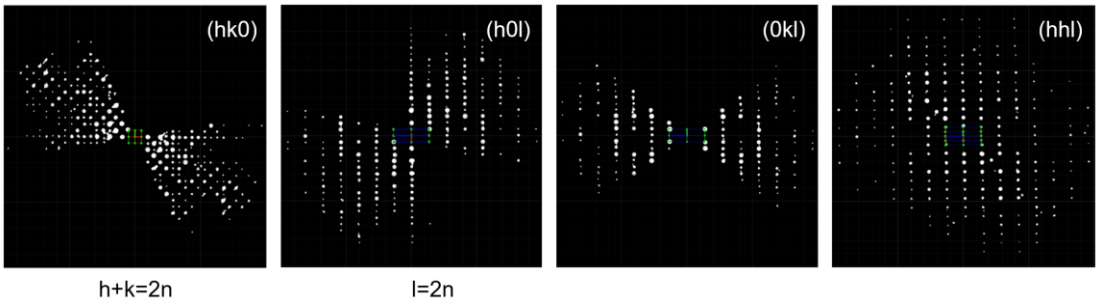

Fig. S29. The 3D reciprocal lattice of CIM-2 reconstructed from the 3DED data. (hk0), (h0l), (0kl) and (hhl) planes are cut from the reconstructed reciprocal lattice, showing the systematic absences.

Table S5. Crystallographic data and structure refinement of CIM-2.

Crystal system	Tetragonal
Space group (number)	$P4_2$ (77)
a [Å]	20.600
b [Å]	20.600
c [Å]	7.360
α [°]	90
β [°]	90
γ [°]	90
Radiation	Electron (λ=0.0197 Å)
2θ range [°]	0.11 to 1.33 (0.85 Å)
Index ranges	$-22 \le h \le 21$ $-24 \le k \le 24$ $-8 \le l \le 8$
Reflections collected	9722
Independent reflections	5053 R_{int} = 0.2774 R_{sigma} = 0.2780
Completeness to θ = 0.664°	95.1 %
Data / Restraints / Parameters	5053/1/403
Goodness-of-fit on F^2	1.023
Final R indexes [I≥2σ(I)]	R_1 = 0.1943 wR_2 = 0.4532
Final R indexes [all data]	R_1 = 0.2291 wR_2 = 0.4966

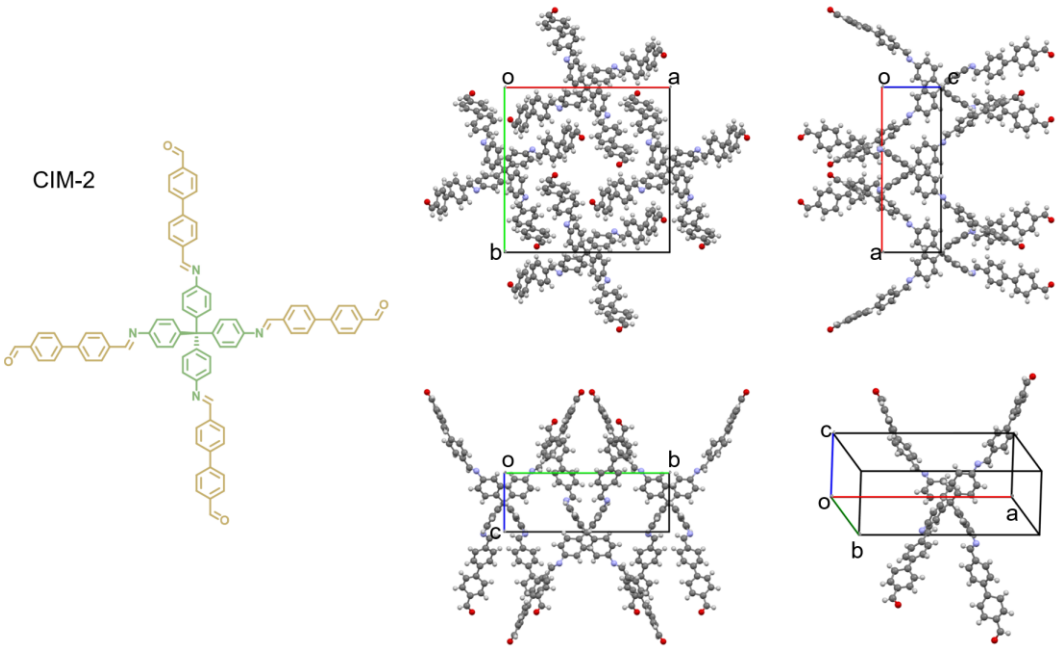

Fig. S30. The crystal structure model of CIM-2 determined from the 3DED dataset collected at 89 K.

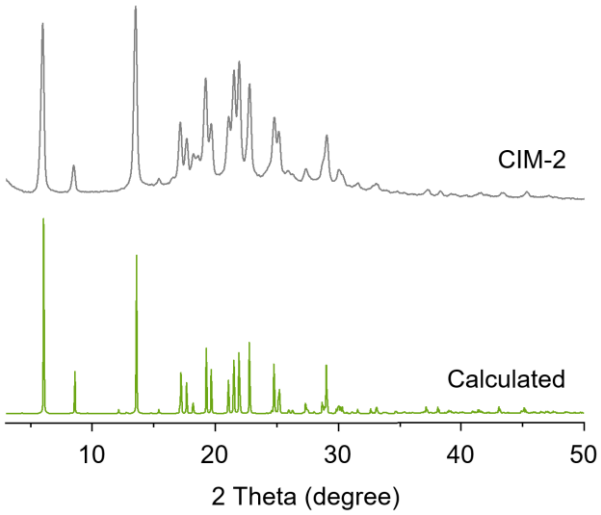

Fig. S31. Comparison of measured PXRD pattern of CIM-2 and simulated one from determined crystal structure by 3D ED, showing the consistent result.

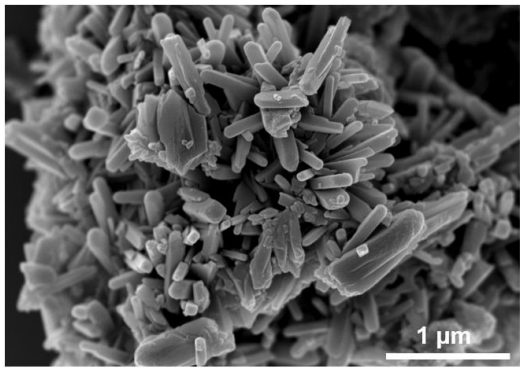

Fig. S32. Scanning electron microscopy image of CIM-2.

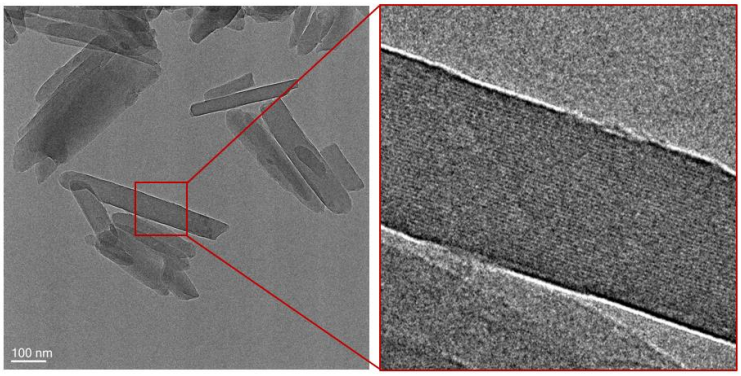

Fig. S33. High resolution transmission electron microscopy image of CIM-2 with the enlarged lattice fringe image showing clear lattice fringes, confirming the long-range ordered structure of CIM-2.

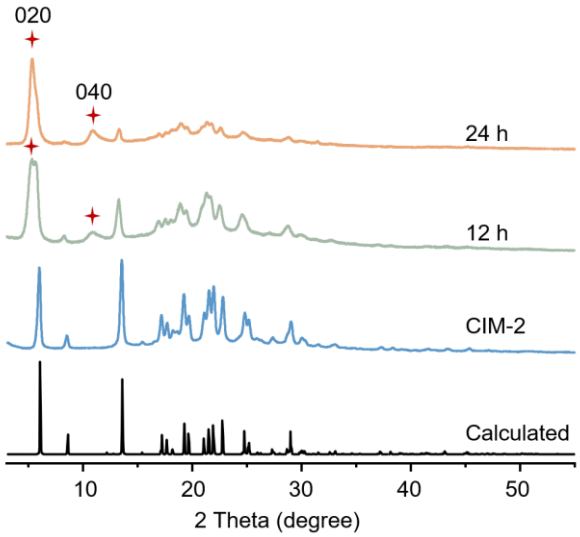

Fig. S34. PXRD patterns corresponding to different heat treatment times during the transformation of CIM-2 into COF-320. The characteristic peaks of the labelled stars are attributed to the (020) and (040) crystal planes of COF-320.

Crystalline intermediate CIM-3 and TJU-300

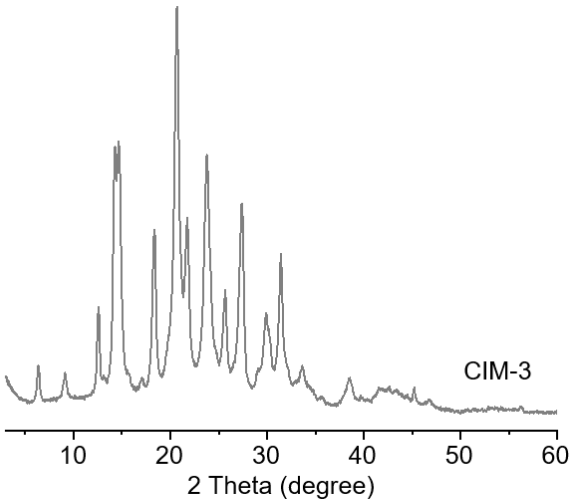

Fig. S35. PXRD pattern of CIM-3 showing good crystallinity.

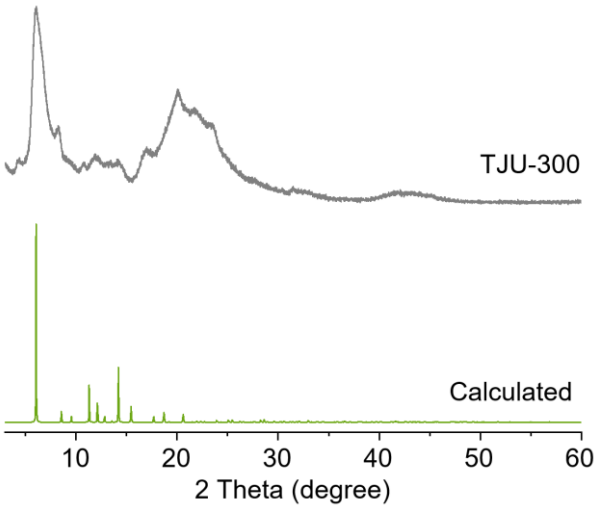

Fig. S36. Comparison of measured PXRD pattern of TJU-300 with the calculated one from simulated structure, showing the consistent result.

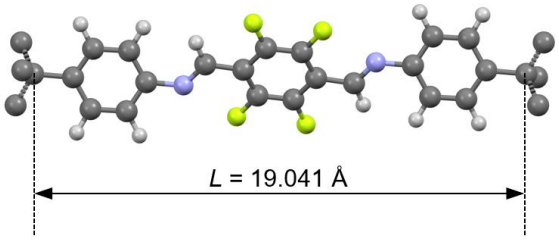

Fig. S37. The length (L) of the organic joint between two tetrahedral nodes from the simulated structure of TJU-300.

Table S6. Crystallographic data of CIM-3 simulated based on the 5-fold interpenetrated dia net.

Crystal system	tetragonal
Space group (number)	$I4_1/a$ (88)
a [Å]	29.204
b [Å]	29.204
c [Å]	9.776
α [°]	90
β [°]	90
γ [°]	90
L [Å]	19.041
N	5.0

Crystalline intermediate CIM-4 and TJU-301

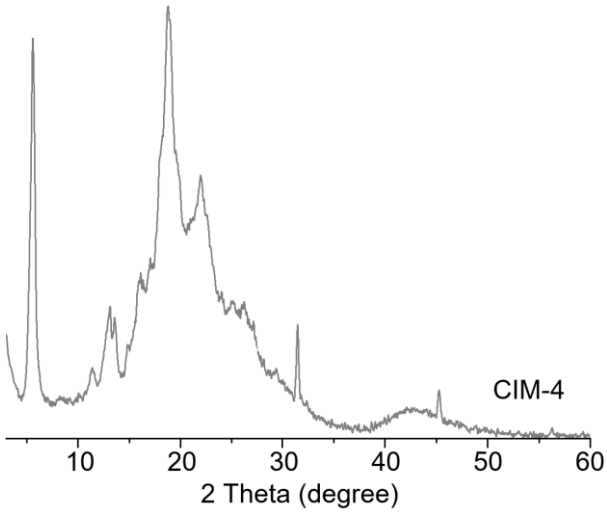

Fig. S38. PXRD pattern of CIM-4.

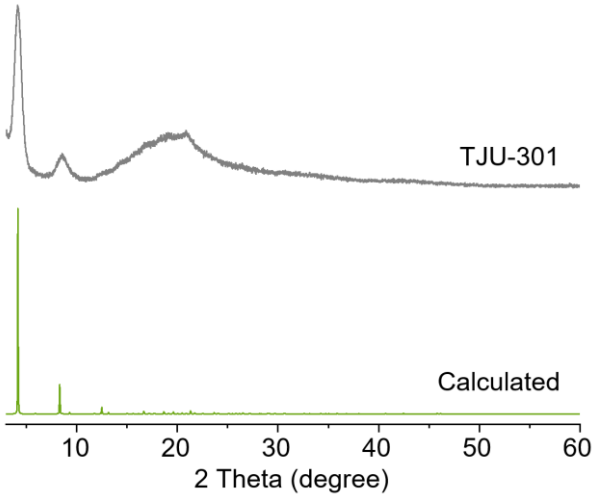

Fig. S39. Comparison of measured PXRD pattern of TJU-301 with the calculated one from simulated structure, showing the consistent result.

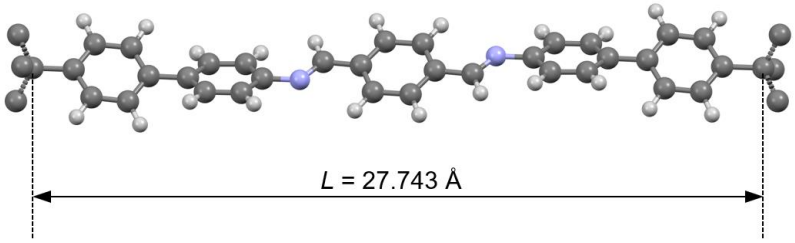

Fig. S40. The length (L) of the organic joint between two tetrahedral nodes from the simulated structure TJU-301.

Table S7. Crystallographic data of CIM-4 simulated based on the 11-fold interpenetrated dia net.

Crystal system	tetragonal
Space group (number)	$I4_1/a$ (88)
a [Å]	42.531
b [Å]	42.531
c [Å]	6.479
α [°]	90
β [°]	90
γ [°]	90
L [Å]	27.743
N	11.0

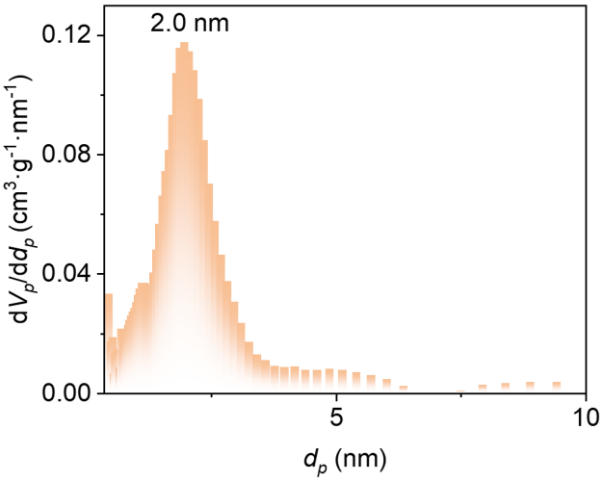

Fig. S41. Pore size distribution histogram of TJU-301 calculated from N_2 adsorption-desorption isotherms at 77 K.

Additional support information

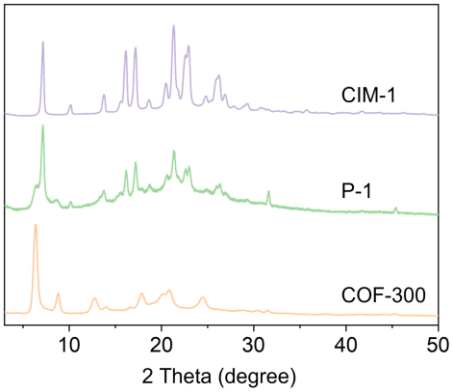

Fig. S42 PXRD patterns of P-1, CIM-1 and COF-300.

Tetrahedral monomer (TAM) is required in the CIM to COFs transformation process. First, the material composition of the starting material and the final product is considered. The molar ratio of tetrahedral monomer to linear monomer for the final product COFs is 1:2, and the molar ratio of tetrahedral monomer to linear monomer for the crystalline intermediates is 1:4. Therefore, 1 mole of tetrahedral monomer is required for every 1 mole of CIM used as a starting feed in the transformation process, which ensures that the composition of the starting feed is the same as that of the final product COFs. COFs have the same composition. We show experimentally that this relative casting is necessary. Conversion of CIM-1 alone under the same conditions gave the product P-1. Comparing its PXRD spectrum with that of CIM-1 and COF-300 derived from CIM-1 and tetrahedral ligand with equal moles of CIM-1 and tetrahedral ligand as feed, P-1 also retained a large number of CIM-1 crystals, suggesting that the crystalline intermediates can be partially converted to COFs but not completely in the absence of tetrahedral amine ligand (Fig. S42). The process also demonstrated the slowly release property of CIM. Furthermore, in the absence of consumed positive promotion in the reaction system, the CIM still maintained a stable crystalline state without decomposition in the mixed solvent system at 90 °C.

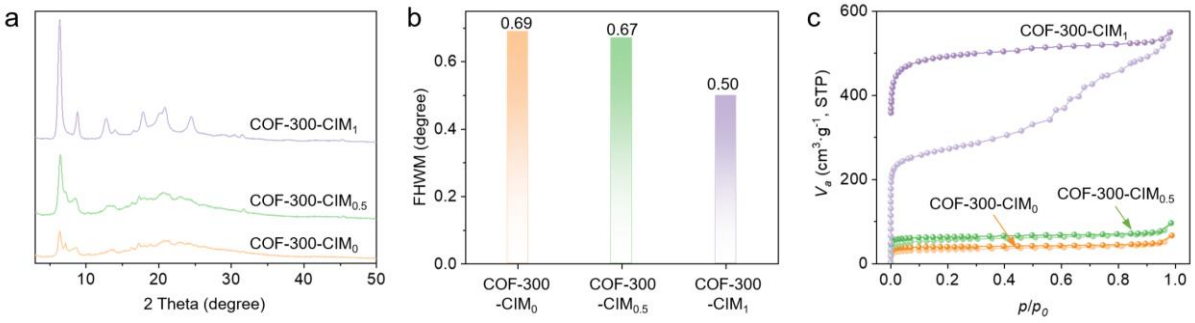

Fig. S43 (a) PXRD patterns, (b) FHWM derived from PXRD patterns and (c) nitrogen adsorption desorption isotherms for COF-300-CIM_0, COF-300-$CIM_{0.5}$ and COF-300-CIM_1. The foot marker in sample name represents the molar ratio of CIM seeds relative to the starting materials.

To further understand the amount of CIM influencing the crystallinity of COF-300, we have conducted additional experiments by varying the molar ration of CIM seeds from 0 to 1 relative to the starting materials. The results are presented in Fig. S43 below.

It is evident that the crystallinity of COF-300 gradually increases with increasing CIM seed amounts (Fig.S43a), which is consistent with the decreasing trend in the FHWM derived from PXRD patterns (Fig. S43b). Among three samples, the value of FHWM of COF-300-CIM_1 is the lowest which suggests the highest crystallinity, followed by COF-300-$CIM_{0.5}$, COF-300-CIM_0. Moreover, nitrogen adsorption-desorption isotherm experiments show that the specific surface areas of COF-300-CIM_0 and COF-300-$CIM_{0.5}$ are 115.11 $m^2 \cdot g^{-1}$ and 193.27 $m^2 \cdot g^{-1}$, respectively, much lower than that of COF-300-CIM_1, 938.09 $m^2 \cdot g^{-1}$(Fig. S43c). Therefore, the amount of CIM seeds will impact the kinetics of transformation process, and the greater CIM seeds add, the higher crystallinity of COFs product will be.

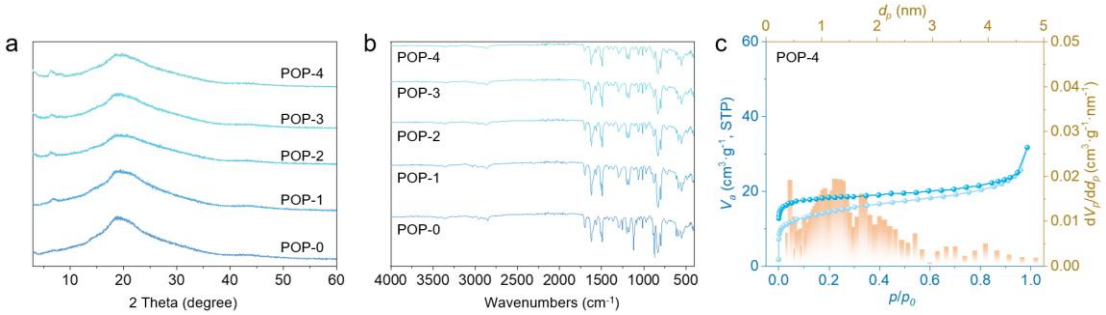

Fig. S44 (a) PXRD mapping and (b) FTIR spectra of POP-0, POP-1, POP-2, POP-3 and POP-4. (c) Nitrogen adsorption-desorption isotherm for POP-4.

To compare the difference of our proposed CIM-to-COFs transformation strategy from the previously reported POP-to-COFs pathway, we have performed addition experiments. Amorphous porous organic polymers (POPs) were prepared mechanochemically without thermal treatment, and then the POP-to-COF transformation experiments were carried out under the same CIM transformation conditions for 0 h (POP-0), 1 h (POP-1), 3 h (POP-2), 6 h (POP-3) and 12 h (POP-4), respectively. PXRD patterns and FTIR spectra of these samples are shown in Figs. S44a and S44b, respectively. Compared with the CIM transformation (Fig. 1b in the manuscript), the phase transformation process from an amorphous POP to crystalline COFs is remarkably slow. There are merely minute amounts of COFs that can be detectable. These results highlight the superiority of CIM transformation on the production of COFs. Besides, the nitrogen adsorption-desorption isotherm experiment of POP-4 sample shows that the porosity of the resultant product is minimal and the calculated value of the specific surface area is only 50.82 $m^2 \cdot g^{-1}$ (Fig. S44c), which is significantly lower than COFs product prepared by CIM transformation (Figs. 1d and 1g in the manuscript).

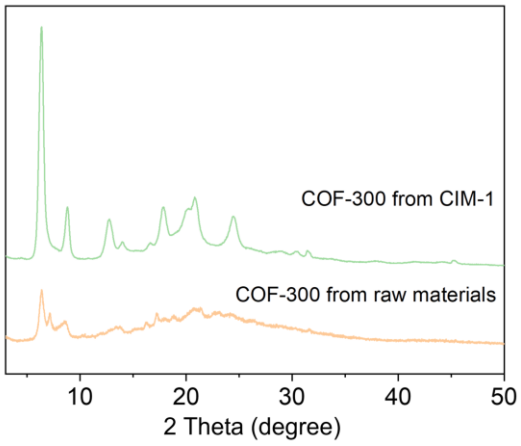

Fig. S45 PXRD patterns for COF-300 from CIM-1 and COF-300 from raw materials.

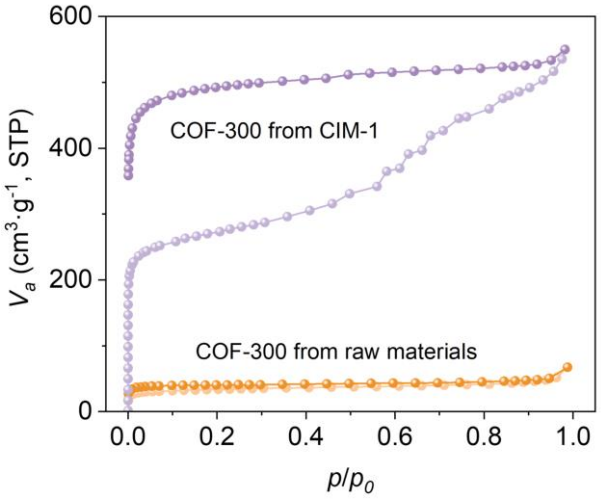

Fig. S46 N_2 adsorption-desorption isotherms of CIM-1 and COF-300 from raw materials.

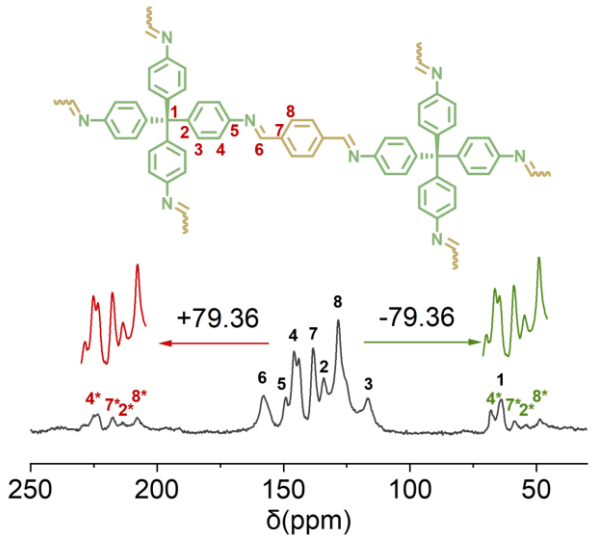

Fig. S47 Solid-state ^{13}C CP-MAS NMR spectrum of COF-300-c5. Note that the asterisks denote the spinning sidebands.

In order to demonstrate the product purity of COFs synthesised by CIM transformation, we also performed solid-state MAS ^{13}C NMR tests on activated COF-300-c5 (Fig. S47). As can be seen from Fig. 1b, the characteristic peaks of COF-300-c5 synthesized by CIM-1 transformation are identical to the structure of the pure product, which is consistent with the results reported by classical solvothermal synthesis (note that the asterisks denote the spinning sidebands).[7] Side bands in solid-state NMR should appear in a symmetrical fashion. In view of this, we have conducted a more detailed analysis on the solid-state ^{13}C CP-MAS NMR spectra of CIM-1 and COF-300 (Figs. 2d and S47), determining the assignments based on the signals from the spectra. These results suggest that the products of COFs synthesised by CIM transformation have the same high purity as those synthesised by solvothermal methods.

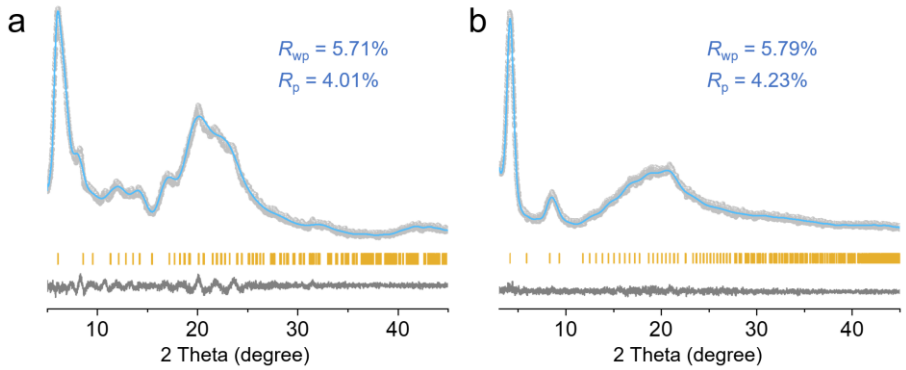

Fig. S47 The Pawley refinement data plots of PXRD of (a) TJU-300 and (b) TJU-301.

The unit cell parameters of TJU-300 and TJU-301 were resolved by the PXRD pattern measurements in conjunction with structural simulations. Geometrical energy minimisation was performed using the Materials Studio software package based on the 5-fold and 11-fold interpenetrated dia net for TJU-300 and TJU-301. The simulated PXRD patterns were in good agreement with the experimental ones (Fig. S47). Furthermore, full profile pattern matching (Pawley) refinements were carried out on the experimental PXRD patterns. The refinement results yield unit cell parameters nearly equivalent to the predictions with good agreement factors (a = b = 29.204 Å, c = 9.776 Å, α = β = γ = 90°, R_{wp} = 5.71% and R_p = 4.01% for TJU-300; a = b = 42.531 Å, c = 6.479 Å, α = β = γ = 90°, R_{wp} = 5.79% and R_p = 4.23% for TJU-301). Finally, we verified the degree of interpenetration (N) between TJU-300 and TJU-301 by simulating the structure to determine the length (L) of the organic linker between the two tetrahedral nodes (Figs. S37 and S40). This value was in perfect agreement with the expected result (Tables S6 and S7). This proves that the simulated structure is reliable.

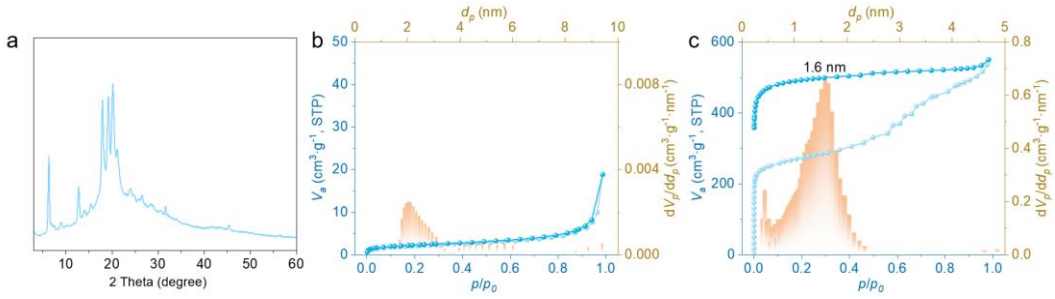

Fig. S48 (a) PXRD pattern of pristine COF-300-c5. (b) Nitrogen adsorption-desorption isotherms of pristine COF-300-c5 and (c) activated COF-300-c5.

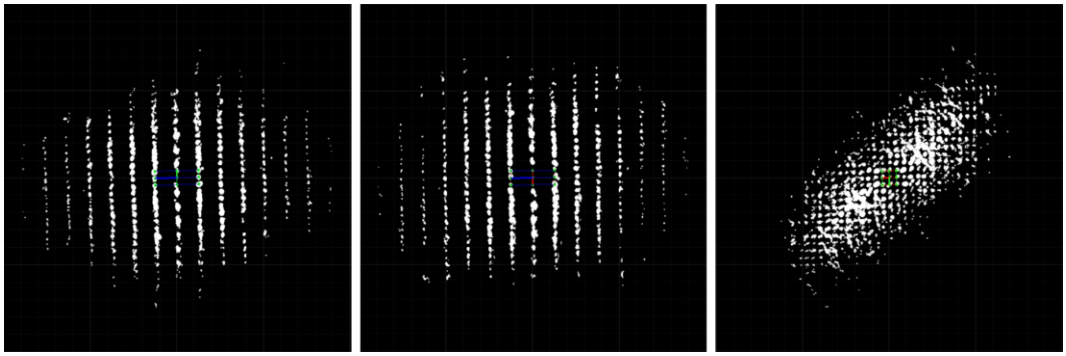

Fig. S49 Reconstructed 3D reciprocal space of CIM-1 viewed along a*, b* and c* axis.

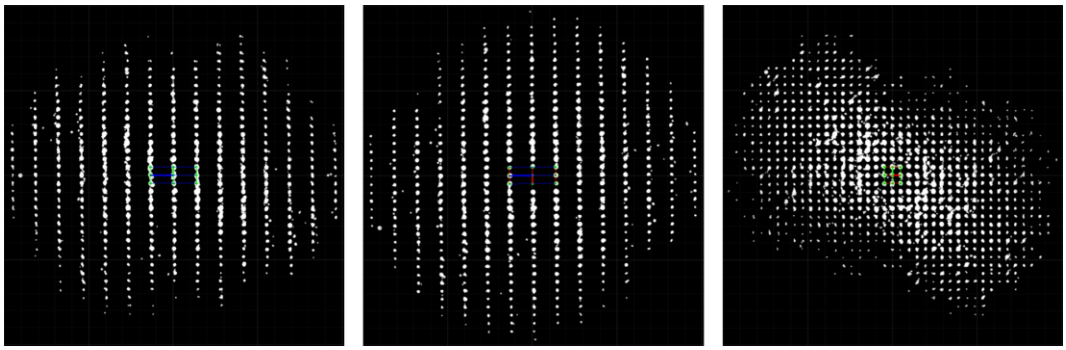

Fig. S50 Reconstructed 3D reciprocal space of CIM-2 viewed along a*, b* and c* axis.

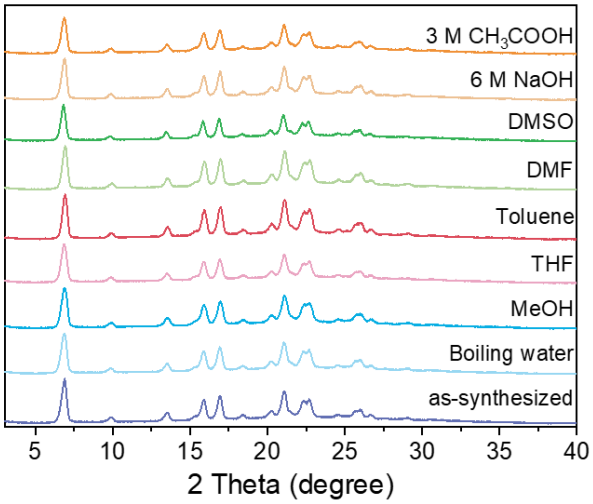

Fig. S51 PXRD patterns of the synthesized CIM-1 after 24 h soaking in different solvents.

To emphasize the advantages of the crystalline intermediate strategy, we evaluated the chemical stability of CIM-1 in various solvents for 24 h (Fig. S51).PXRD analysis showed that CIM-1 exhibited excellent stability and maintained crystallinity in various solvents such as boiling water, methanol (MeOH), tetrahydrofuran (THF), toluene, N,N-dimethylformamide (DMF), dimethyl sulfoxide (DMSO), alkaline aqueous solution and glacial acetic acid aqueous solution exhibited excellent stability and maintained

crystallinity in various solvents and still retained their structural integrity, probably due to the absence of solvent molecules in its framework.

References

1 Uribe-Romo, F. J. *et al.* A Crystalline Imine-Linked 3-D Porous Covalent Organic Framework. *Journal of the American Chemical Society* **131**, 4570-4571, doi:10.1021/ja8096256 (2009).

2 Chen, Y. *et al.* Guest-Dependent Dynamics in a 3D Covalent Organic Framework. *Journal of the American Chemical Society* **141**, 3298-3303, doi:10.1021/jacs.8b13691 (2019).

3 Wang, X.-L. *et al.* Facile Solution-Refluxing Synthesis and Photocatalytic Dye Degradation of a Dynamic Covalent Organic Framework. *Molecules* **27**, 8022, doi:10.3390/molecules27228002 (2022).

4 Wang, X.-L. *et al.* Dynamic Imine Exchange Reactions for Facile Synthesis of Imine-Linked Covalent Organic Frameworks. *Chemistry of Materials* **35**, 10070-10077, doi:10.1021/acs.chemmater.3c02092 (2023).

5 Zhou, Z. *et al.* Growth of single-crystal imine-linked covalent organic frameworks using amphiphilic amino-acid derivatives in water. *Nature Chemistry* **15**, 841-847, doi:10.1038/s41557-023-01181-6 (2023).

6 Ma, T. *et al.* Single-crystal x-ray diffraction structures of covalent organic frameworks. *Science* **361**, 48-52, doi:10.1126/science.aat7679 (2018).

7 *Ma, T. et al.* Observation of Interpenetration Isomerism in Covalent Organic Frameworks. *Journal of the American Chemical Society **140**, 6763-6766.* doi: 10.1021/jacs.8b03169 (2018).